

Testing inhomogeneous cosmography in our cosmic neighborhood using CosmicFlows-4

S. M. Koksbang^{1, *}

¹*CP³-Origins, University of Southern Denmark, Campusvej 55, DK-5230 Odense M, Denmark*

The convergence of the general cosmographic expansion of the luminosity distance is studied in a model of our cosmic neighborhood based on publicly available density and velocity fields obtained from CosmicFlows-4 data. The study confirms earlier findings that indicate divergence of the general cosmographic expansion at low redshifts, well before $z \sim 0.1$. By being based on a realistically placed observer in a semi-realistic model constructed from a real map of our local cosmic neighborhood, the presented results firmly establish that the range of convergence must be an important focus when using the general cosmographic expansion. The study also highlights the loss of information we face when using the traditional cosmographic expansion based on the Friedmann-Lemaître-Robertson-Walker models. Specifically, sky maps of effective Hubble, deceleration, jerk and curvature parameters showing strong fluctuations of these across the sky are presented. These fluctuations and their meaning cannot be established using the simple framework of standard cosmology. It is suggested that the general cosmographic expansion should be studied at higher order and in recast forms in order to scrutinize the possibility of obtaining convergence at higher redshift. In addition, the general cosmographic expansion in its current form may have faster rate of convergence when applied to other datasets. It is therefore suggested that the use of general cosmographic expansions should generally be accompanied by realistic assessments of the expansion's precision for the given dataset studied, e.g. by employing the modeling procedure used here to make a synthetic model universe based on the data.

Lastly, it is important to stress that a poor convergence does not necessarily mean that the information extracted by fitting data to the general cosmographic expansion is useless. It simply means that we must be careful when interpreting the results and e.g. include considerations of what scales the expansion coefficients are probing.

I. INTRODUCTION

The Λ CDM model is the onset for interpreting observations in standard cosmology. However, observational data has become so ample and precise that fluctuations in observations across the sky can be studied for a variety of observables. An interesting example is the recent array of studies into the anisotropy of the Hubble diagram [1–9] (see e.g. [10] for an overview of the results of these studies and [11] for a review). These studies illustrate the high precision of current observational data, demonstrating that observational cosmological data has reached a level of detail that permits us to thoroughly study its anisotropy and inhomogeneity. Additionally, in recent years, observational challenges for the standard Λ CDM model have appeared. A striking but somewhat overlooked example is an apparent disagreement between the dipole anisotropy of the cosmic microwave background and other distant sources [12–14] (see e.g. [15] for the background for these studies).

Overall, one may argue that the time has come to go beyond the standard framework of employing Friedmann-Lemaître-Robertson-Walker (FLRW) cosmology when interpreting observations. This is further supported by studies such as [16] showing strong tension between the local universe with the Λ CDM model. Such studies may indicate that the Λ CDM model and the corresponding

standard tools for data analysis simply are not accurate enough to be used with modern astrophysical data, especially when considering low-redshift observations.

Fittingly, there has been an increased activity among cosmologists in developing formalisms for taking anisotropy and inhomogeneity into account in data analyses. A prime example is the cosmographic expansion of the luminosity distance for a general spacetime presented in [17]¹, which has recently been augmented in the series [19–21] and which builds on earlier work such as [22–24]. The formalism of [17] has been used in studies based on numerical relativity [25, 26] and in N-body simulations based on the weak-field approximation [27]. The formalism has even been used in relation to studying real data in e.g. [3, 10]. However, already in [25, 26] it was noticed that the general cosmographic framework may have an obstacle in terms of a very low radius of convergence (or at least a very slow convergence rate). Indeed, good convergence at third order for redshifts up to $z \approx 0.1$ was only obtained in simulations with a smoothing scale as large as 200Mpc/h. The obstacle was further confirmed in [28] where the convergence of the general cosmographic expansion was studied in various Lemaître-Tolman-Bondi (LTB) [29–31] models constructed to resemble our cosmic neighborhood. This study made it clear that the convergence of the underlying Taylor expansion of the general

* koksbang@cp3.sdu.dk

¹ Some of the results presented in [17] were earlier derived in the PhD thesis [18].

cosmographic expansion depends strongly on the local environment and that assessments stating that the expansion is suitable up to around $z = 0.1$ (as in e.g. [21]) are simply too optimistic.

The studies listed above *indicate* that the general cosmographic expansion only converges at redshifts much lower than $z = 0.1$ unless structures are radically smoothed or expansion terms far beyond third order are included. Firmly establishing realistic limits of the convergence will, however, require detailed and realistic models of our cosmic neighborhood. The goal here is to make exactly such a model and place realistic limits on the convergence of the general cosmographic expansion of the luminosity distance. More precisely, the objective here is to study the convergence of the general cosmographic expansion devised in [17], using two versions of a model of our local universe based on real observations combined with a weak-field approximation. The first section below presents the constructed models of our local universe in detail. Following that, Section III provides an overview of the formalism used to calculate the redshift-luminosity distance relation and cosmographic expansion for the model. Section IV presents the results from a numerical investigation based on the models, while Section V provides a summary and conclusions.

II. MODEL SETUP

This section serves to introduce the model that will be studied in the later sections. The goal is to construct a realistic model of the local universe so that the model can be used to realistically estimate the radius of convergence of the general cosmographic expansion of the luminosity distance. Two versions of the overall same model will be considered.

The realistic models are obtained by using the density and peculiar velocity fields presented in [32] based on the CosmicFlows-4 data [33]. The CosmicFlows-4 dataset contains distance and redshift measurements of nearly 56,000 galaxies in our local cosmic neighborhood. Corresponding peculiar velocities can be extracted from the data by assuming a background FLRW model (see e.g. [34] for a discussion of this approach). Density fields can then be estimated based on perturbative expressions. This was done in [32], with the resulting density and velocity fields being made publicly available². Two versions of the density and velocity fields are available: a grouped and ungrouped version. In the “ungrouped” dataset, the fields are determined based on each individual galaxy. In the “grouped” dataset, the galaxies are bunched into $\sim 38,000$ groups from which average velocity and density fields are determined (see e.g. [35]

for details on the grouping procedure). To assess the robustness of the results presented in Section IV, models based on both these datasets will be considered. Figure 1 shows the density contrast $\delta := \rho/\rho_{\text{bg}} - 1$ and the peculiar velocity field for each model in a 2-dimensional slice going through (SGX, SGY, SGZ) = (0, 0, 0) (our position in supergalactic (SG) coordinates). As discussed in [32], the data is based on the flat Λ CDM model as the background with $\Omega_{m,0} = 0.3$ and $H_0 = 74.6 \text{ km/s/Mpc}$, with the Hubble constant value being equal to the one extracted from the CosmicFlows-4 data in [33]. This is the background model assumed here, but note that smaller variations of H_0 are not crucial for the results presented further below.

Spacetimes based on these density and velocity fields will be constructed by introducing a weak-field approximation inspired by [36]. For this, it is assumed that our local spacetime can be approximated by the perturbed FLRW line element in Newtonian gauge (considering only scalar perturbations)

$$ds^2 = -c^2(1 + 2\Phi)dt^2 + a^2(1 - 2\Phi)(dx^2 + dy^2 + dz^2). \quad (1)$$

It was argued in [37] that a Newtonian N-body simulation can be mapped into a perturbed FLRW spacetime by applying the above line element and combining it with the 4-velocity $u^\mu \propto (1, v^i)$, where v^i is the peculiar velocity field obtained from the simulation. The metric perturbation Φ is then obtained from the density field of the simulation through the Poisson equation, $\nabla^2\Phi = 4\pi G a^2(\rho - \rho_{\text{bg}})$. This method has e.g. been found to apply well to LTB models reproduced with Newtonian N-body simulations [38, 39]. A similar mapping will be used here, using the peculiar velocity field and density contrast from the CosmicFlows-4 data instead of simulation data. The spacetime will be considered using the weak field approximation, only keeping the leading order terms. Following Table 1 of [36] we will thus neglect terms containing the potential except its second order spatial derivatives which are kept at linear order. The density contrast (proportional to the second derivative of the metric potential) and the peculiar velocity field and its derivatives are also kept at linear order.

The velocity and density data of [32] is given on the interval $[-500, 500] \text{ Mpc/h}$ on a 64-point grid in each direction. To obtain a smooth space, we will interpolate using trilinear interpolation between grid points.

The resulting model of our local cosmic neighborhood is clearly only approximate. One may for instance notice that the density contrast becomes smaller than -1 in Figure 1, indicating a negative density field which is obviously un-physical. A density contrast below -1 is also seen in Figure 2 of [32] and is presumably due to a breakdown of the linear approximation used to go from peculiar velocity field to density contrast. However, the negative density does not have any significant

² The data can be found at <https://projets.ip2i.in2p3.fr/cosmicflows/>.

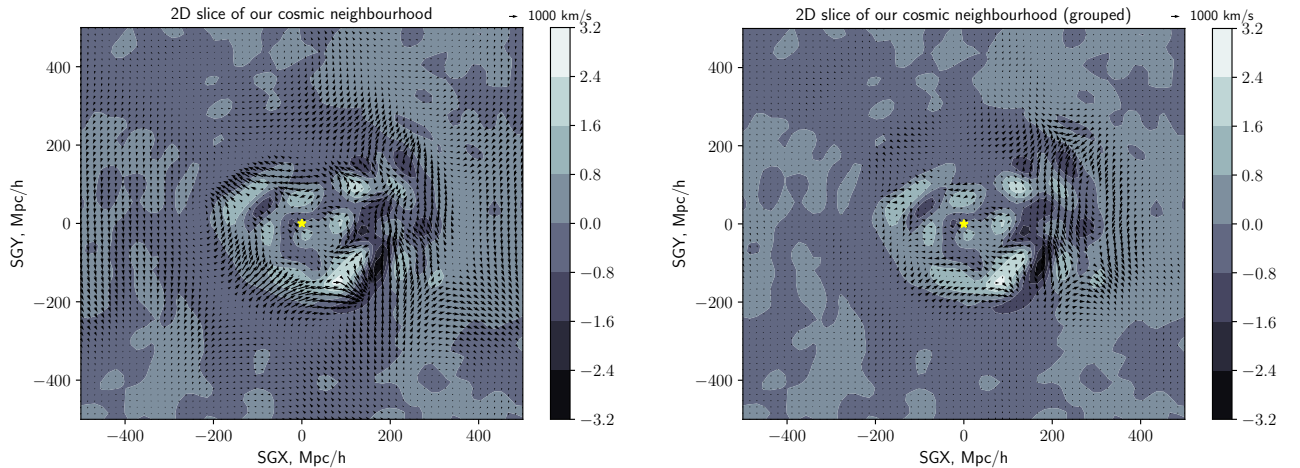


FIG. 1. Two-dimensional slice of model universe corresponding to the middle plot in figure 2 of [32]. A star indicates our position at supergalactic coordinates $(SGX, SGY, SGZ) = (0,0,0)$. The plot to the left shows the slice for ungrouped data while the plot to the right shows the fields for the grouped data.

consequences for the results (viz. no striking effects occur when comparing results along light rays that go through regions with negative density compared to light rays propagating through positive density only).

A further approximation comes into the model from the uncertainty of distance measures which for the CosmicFlows-4 data typically have an error of $\sim 15\%$. This error propagates into the density and peculiar velocity estimates as discussed in e.g. [33, 34]. These uncertainties will not be taken into account here since it is expected that a 15 % change in the fields will not make a significant difference regarding the overall conclusions.

Lastly, it is worth noting that the model as described so far does not include considerations of time-dependence. Since the region probed by the CosmicFlows-4 data is fairly small and light will only be propagated to $z = 0.1$ in the following, the time evolution can largely be ignored and the supergalactic grid described above will be considered a purely spatial grid, although the small time evolution occurring along light rays is automatically taken (roughly) into account on this grid. In the following section, explicit time derivatives of the velocity field will, however, be required. These will be estimated from Euler's equation, taking only the Hubble drag into account, i.e. $v_{,t}^i$ is estimated as $v_{,t}^i \approx -Hv^i$. One can similarly use linear perturbation theory to estimate a time dependence for the density contrast as $\delta_{,t} = -\delta\Theta \approx -\partial_i v^i$ (see e.g. chapter 10 in [40]), where $\delta\Theta$ is the fluctuation in the local expansion rate and the second equality is valid to first order in the weak-field approximation used here. Appendix B serves to demonstrate that the results presented further below do not depend significantly on whether or not the peculiar velocity and density contrast are explicitly evolved according to these equations when

ray tracing.

It is not the claim that the resulting model constitutes an exact replica of our local neighborhood. The model is merely an approximation of our local universe, expected to be realistic and detailed enough to capture the dominant characteristics of the redshift-distance relation and corresponding cosmographic expansions realistically through ray tracing.

III. LIGHT PROPAGATION IN THE LOCAL UNIVERSE MODEL

This section serves to introduce the formalism used for ray tracing through the model universe as well as specifying the utilized general cosmographic expansion.

A. Cosmographic expansion

Using a Taylor expansion in the redshift, the luminosity distance can be written as

$$D_L \approx D_L^{(1)} z + D_L^{(2)} z^2 + D_L^{(3)} z^3, \quad (2)$$

where the expansion coefficients $D_L^{(i)}$ depend on the chosen cosmological model. Following [17] we will define generalized versions of the Hubble (\mathcal{H}), deceleration (\mathcal{Q}) and jerk (\mathcal{J}) parameters and a generalized spatial curva-

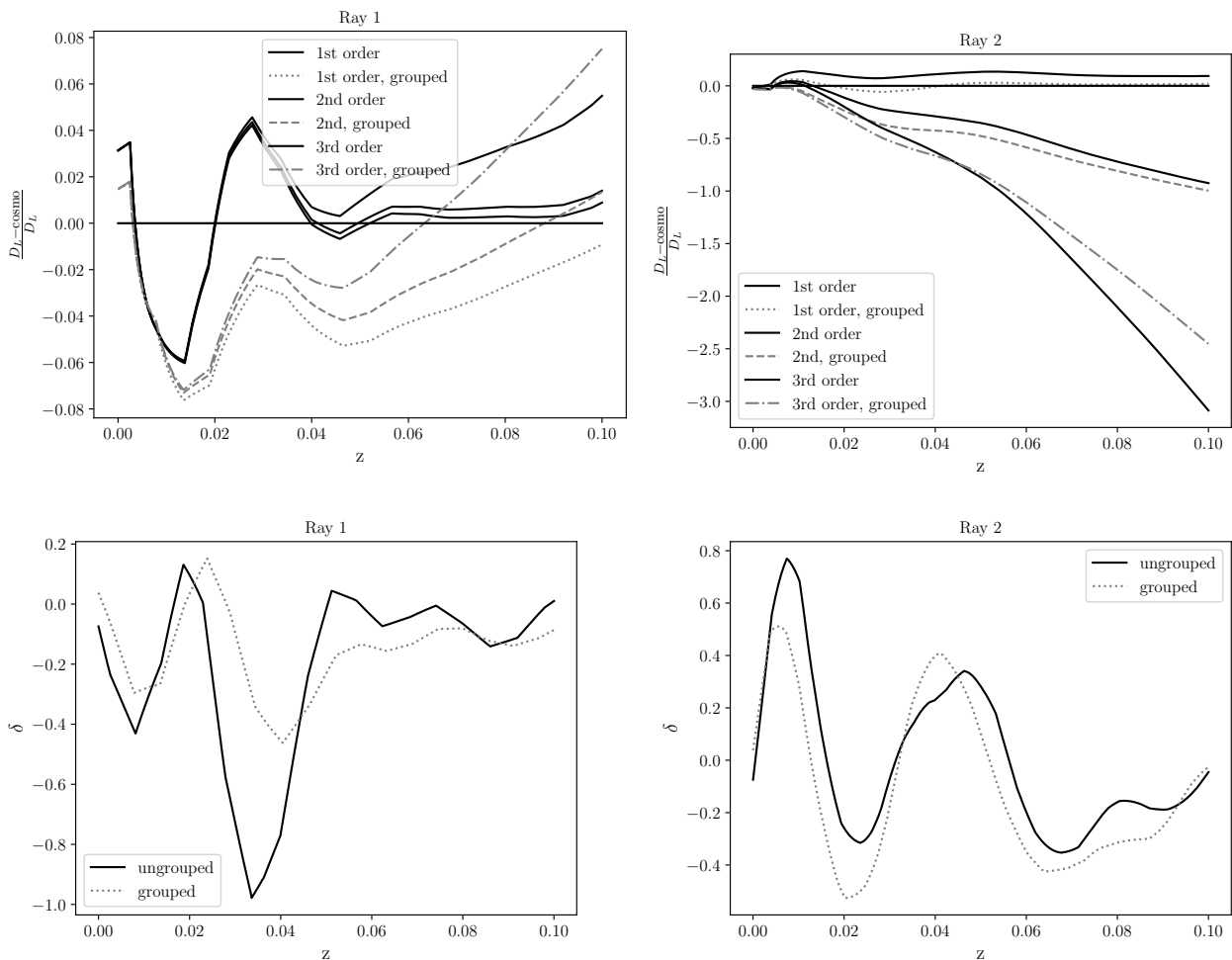


FIG. 2. Density contrast and relative deviations between exact redshift-distance relation and cosmographic expansions (denoted as “cosmo”) along two fiducial lines of sight.

ture term (\mathcal{R}). These are given by

$$\begin{aligned}
 \mathcal{H} &= \frac{1}{3}\Theta + e^\mu e^\nu \sigma_{\mu\nu} - \frac{e^\mu a_\mu}{c} \\
 \mathcal{Q} &= -1 - \frac{c^2}{E\mathcal{H}^2} \frac{d\mathcal{H}}{d\lambda} \\
 \mathcal{R} &= 1 + \mathcal{Q} - \frac{c^4}{2E^2} \frac{k^\mu k^\nu R_{\mu\nu}}{\mathcal{H}^2} \\
 \mathcal{J} &= \frac{c^4}{E^2\mathcal{H}^3} \frac{d^2\mathcal{H}}{d\lambda^2} - 4\mathcal{Q} - 3,
 \end{aligned} \tag{3}$$

where $e^\mu = u^\mu/c - ck^\mu/(-u_\alpha k^\alpha)$ is the spatial direction vector of the light ray as seen by an observer comoving with the dust, $\sigma_{\mu\nu}$ is the shear tensor and Θ the expansion rate of the matter. $E = -u^\alpha k_\alpha$ is the energy in the matter frame, and $a^\mu = u^\nu \nabla_\nu u^\mu$ is the 4-acceleration of the matter. Their explicit expressions in the models considered here are shown in Appendix A. For the results shown in Section IV, the derivatives $d\mathcal{H}/d\lambda$ and $d^2\mathcal{H}/d\lambda^2$ were computed numerically using forward finite differences along the light rays.

It was in [17] shown that the coefficients of the cosmographic expansion for a general spacetime can be written as

$$\begin{aligned}
 D_L^{(1)} &= \frac{c}{\mathcal{H}_O} \\
 D_L^{(2)} &= c \frac{1 - \mathcal{Q}_O}{2\mathcal{H}_O} \\
 D_L^{(3)} &= c \frac{-1 + 3\mathcal{Q}_O^2 + \mathcal{Q}_O - \mathcal{J}_O + \mathcal{R}_O}{6\mathcal{H}_O},
 \end{aligned} \tag{4}$$

assuming that the redshift is monotonous along the light ray, and where subscripted \mathcal{O} 's indicate evaluation at the observer.

B. Ray tracing

To compute the redshift-distance relation using the simple model of our cosmic neighborhood introduced in Section II, we must solve the geodesic equations. Since the metric scalar perturbation and its first derivatives are

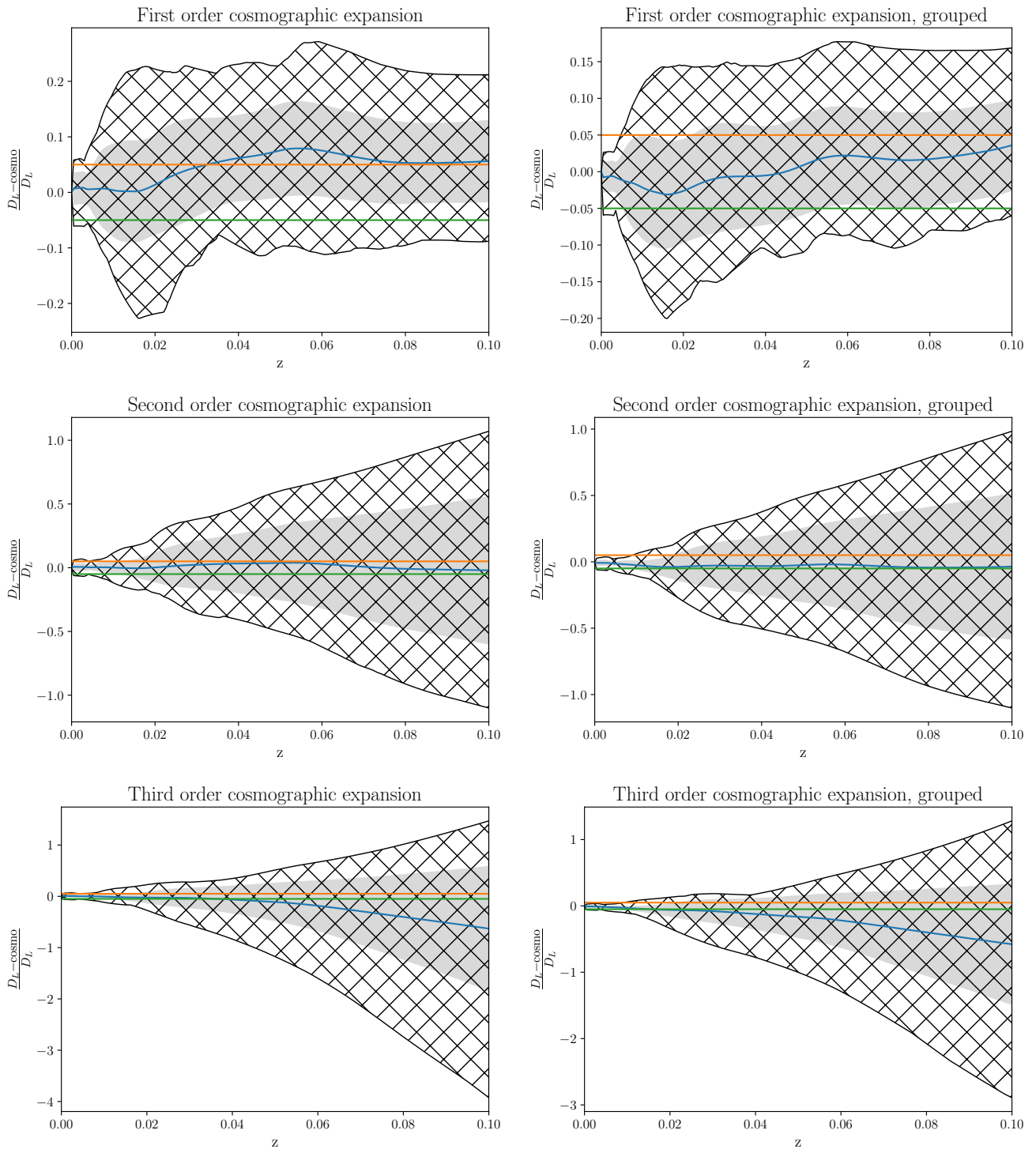


FIG. 3. Relative deviation between the exact luminosity distance (D_L) and the cosmographic expansion (“cosmo”) at first, second and third order. Hatched areas show the fluctuation along all light rays while the shaded area shows a standard deviation around the mean which is also plotted and appears as the slightly curving line in the plots. To ease interpreting the plots, the figures include lines at $\pm 5\%$. The figures to the left show results for the model based on the ungrouped data while the figures to the right show the results for the model based on the grouped data.

neglected, the geodesic equations are simply those of the FLRW metric which we can write as

$$\begin{aligned}\frac{dk^t}{d\lambda} &= -H(k^t)^2 \\ \frac{dk^i}{d\lambda} &= -2Hk^i k^t.\end{aligned}\quad (5)$$

The luminosity distance, D_L , is obtained from the angular diameter distance, D_A , through the reciprocity relation. The angular diameter distance is computed as the square root of the determinant of the distortion matrix, D . The distortion matrix is obtained by solving the transport equation

$$\frac{d^2 D}{d\lambda^2} = TD, \quad (6)$$

where T is the tidal matrix with components based on $\mathbf{R} = -1/2R_{\mu\nu}k^\mu k^\nu$ and $\mathbf{F} = -1/2C_{\alpha\beta\gamma\mu}(\epsilon^*)^\alpha k^\beta (\epsilon^*)^\gamma k^\mu$ according to

$$T = \begin{pmatrix} \mathbf{R} - \text{Re}(\mathbf{F}) & \text{Im}(\mathbf{F}) \\ \text{Im}(\mathbf{F}) & \mathbf{R} + \text{Re}(\mathbf{F}) \end{pmatrix}. \quad (7)$$

The transport equation is solved simultaneously with the geodesic equations and the parallel transport equation of the screen space basis vectors E_1^μ, E_2^μ which are orthogonal to each other as well as k^μ and the observer velocity u^μ ³. The screen space basis vectors are combined into $\epsilon^\mu = E_1^\mu + iE_2^\mu$ when computing \mathbf{F} . However, the Weyl contribution to the angular diameter distance may be dropped since we are only interested in the dominant contributions to the distance fluctuations given by the gravitational and Doppler convergence, which are encapsulated already in \mathbf{R} and the redshift $1+z = (u^\mu k_\mu)|_e / (u_\alpha k^\alpha)|_o$. Indeed, at low redshift, we can even neglect the gravitational convergence and only consider the Doppler convergence (see e.g. [39, 41, 42] for discussions and demonstrations of this point). The results presented in the next section were obtained by considering both the Doppler and gravitational convergence, but it has been verified that the gravitational convergence indeed is subdominant and that the results and conclusions presented below are unchanged if the gravitational convergence is neglected. For the model spacetime we have

$$\mathbf{R} = -\frac{4\pi G\rho}{c^4} (u^\mu k_\mu)^2. \quad (8)$$

IV. NUMERICAL RESULTS

In this section, we present results from propagating light rays through the two versions of the model of our

cosmic neighborhood presented in Section II. Before presenting statistical results based on a large number of light rays, it is prudent to consider a few individual light rays. Figure 2 therefore shows the cosmographic expansion relative to the exact redshift-distance relation along two selected light rays in both models. The two light rays were selected because they demonstrate two different, important points. The plots to the left show the results from a light ray along which the deviation between the exact and cosmographic results remain fairly small for the entire studied redshift interval. There are noticeable deviations between the exact and cosmographic expansions but they are only of a few percent and do not grow significantly along the light ray, until at $z \approx 0.05$. These deviations are therefore expected to largely represent lack of precision of the model, i.e. imprecision due to computing derivatives using finite-difference formulas, linear interpolations on the grid, and neglecting higher-order terms. The plots to the right in figure 2 show a very different behavior. In these plots, the deviation between the cosmographic expansion and the exact redshift-distance relation grows strongly with the redshift. Along this line of sight it is clear that the cosmographic expansion breaks down long before $z = 0.1$ is reached. The figure to the left might similarly be revealing the beginning of divergence of the cosmographic expansion for $z \geq 0.05$, where the deviation between the exact redshift-distance relation and the cosmographic expansions seem to begin to grow. The results are very similar for the grouped versus ungrouped model.

Figure 2 also shows the density contrasts along the corresponding light rays. From this, it is clear that the density contrast has a much steeper gradient near the observer along the light ray where the cosmographic expansion most clearly seems to break down. It is not surprising that such strong gradients lead to a significantly reduced radius of convergence or slow convergence rate of a Taylor expansion. Table I shows the expansion coefficients for the four light rays. The table also shows the fractions of the coefficients. These are included in the table because the radius of convergence, R , can be computed as $R = \lim_{n \rightarrow \infty} |a_n/a_{n+1}|$, where a_n are the coefficients of the expansion.

Comparison of Table I and Figure 2 reveals that the diverging cosmographic expansion appears along the line of sight where $D_L^{(3)}$ is about one order of magnitude larger than $D_L^{(2)}$ which again is one order of magnitude larger than $D_L^{(1)}$. In this case, the third order of the Taylor expansion begins to dominate over the first order expression when $z \approx \sqrt{D_L^{(1)}/D_L^{(3)}} \approx 0.065$ (using values for the ungrouped model). This value is clearly too optimistic when compared with Figure 2 where the divergence appears to begin already at $z \approx 0.0075$. We can understand this simply as a reminder that the true radius of convergence cannot be estimated without including more expansion coefficients. This is also indicated by the coefficient frac-

³ As discussed in [43], we may assume an arbitrary velocity field here and thus that the 4-velocity orthogonal to the screen space basis vectors is parallel transported along the light rays. Assuming this, we can obtain the basis vectors along the light rays by parallel transporting them along the null geodesics.

Model	$D_L^{(1)}$	$D_L^{(2)}$	$D_L^{(3)}$	$ D_L^{(1)}/D_L^{(2)} $	$ D_L^{(2)}/D_L^{(3)} $
Ray 1, ungrouped	$42 \cdot 10^2$	$22 \cdot 10^1$	$-19 \cdot 10^3$	19	0.011
Ray 1, grouped	$43 \cdot 10^2$	$-12 \cdot 10^1$	$-22 \cdot 10^3$	36	0.0055
Ray 2, ungrouped	$39 \cdot 10^2$	$22 \cdot 10^3$	$94 \cdot 10^4$	0.22	0.024
Ray 2, grouped	$42 \cdot 10^2$	$44 \cdot 10^3$	$67 \cdot 10^4$	0.097	0.066

TABLE I. Expansion coefficients of two selected light rays in the grouped and ungrouped models. The fractions of neighboring coefficients are also shown.

tions in Table I; to estimate the radius of convergence, the fractions would first need to converge towards a specific value which clearly has not happened in Table I.

The same caveat remains for light ray 1 where we also cannot reliably estimate the radius of convergence. One may nonetheless note that for this line of sight, the third order term is of the same order of magnitude as the first order term, when $z \approx \sqrt{D_L^{(1)}/D_L^{(3)}} \approx 0.46$ (again using data for the ungrouped model). This is an order of magnitude larger than the estimate for light ray 2 which is in agreement with the fact that the divergence happens at lower redshift along light ray 2 than along light ray 1.

Since we cannot make a mathematically precise estimate of the radius of convergence, it is not possible to determine whether the problem actually is a very small radius of convergence or if it is merely a very slow rate of convergence. In the latter case, a better agreement between the cosmographic expansion and the exact redshift-distance relation would simply be achieved by adding more terms to the cosmographic expansion. Either way, it is important to understand if the divergence of the cosmographic expansion seen along ray 2 is common or an outlier when considering many lines of sight. This question is studied in the following subsection.

A. Multiple light rays

This subsection presents the results obtained by propagating 768 light rays in each model. All lines of sight are based on a single observer, namely the one placed at the center of the super galactic coordinate system of the two models. Rather than choosing random lines of sight, the light rays are based on a Healpix⁴ distribution over the sky.

Figure 3 shows the deviations between the exact luminosity distance versus the first, second and third order cosmographic expansions along all lines of sight for both models. For the model based on the ungrouped data, the maximum fluctuations are quite large (above 5 – 10%) already at very low redshifts $z \sim 0.005 - 0.01$. Only considering one standard deviation around the

mean (very) roughly halves the amplitude of the scatter. In addition, as already discussed when considering individual light rays above, the precision of the numerical investigation is quite low and a 5 % error should not be considered particularly problematic as it can simply be due to using the finite difference on a very crude grid space combined with linear interpolation. The important results appear when considering the second and third order expansions where the deviations from the exact redshift-distance relation increase very rapidly and become of order 50 – 100% before $z \approx 0.05$. These values are approximately halved when only considering one standard deviation around the mean. For the third order cosmographic expansion, the mean even seems to diverge, indicating that the lines of sight with divergent cosmographic expansions dominate the statistical results. This is in line with the skewness seen in the figure which shows that the divergence typically is such that the cosmographic expansion is larger than the exact luminosity distance.

The plots obtained from the model based on the grouped data overall shows the same trends as the results obtained for the ungrouped data. The most noticeable deviations between the results obtained from the two models are for the first order cosmographic expansion. Here, the deviation between the first order expansion and the exact redshift-distance relation are still clearly visible for the grouped model, but the deviation are strictly below 10% when only considering one standard deviation of the light rays. Most importantly, however, the divergence of the mean for the third order expansion is still clear for the grouped model, and the mean seems still to be dominated by light rays along which the cosmographic expansion diverges.

All-sky maps showing the relative deviations between the third order cosmographic expansion and the exact redshift-distance relation at different redshifts are presented in figures 4 and 5 for the ungrouped and grouped data, respectively. For the model based on the ungrouped data, especially the $z \approx 0.002$ map shows similar order of magnitudes of the amplitudes and distributions in negative and positive deviations. At $z \approx 0.005$, the amplitude of the deviations is around 5% and the deviations are thus small enough to simply be due to numerical inaccuracy. At higher redshift, the deviations are less symmetric and are pushed towards the negative along a dominant number of lines of sight.

⁴ <https://healpix.sourceforge.io/>

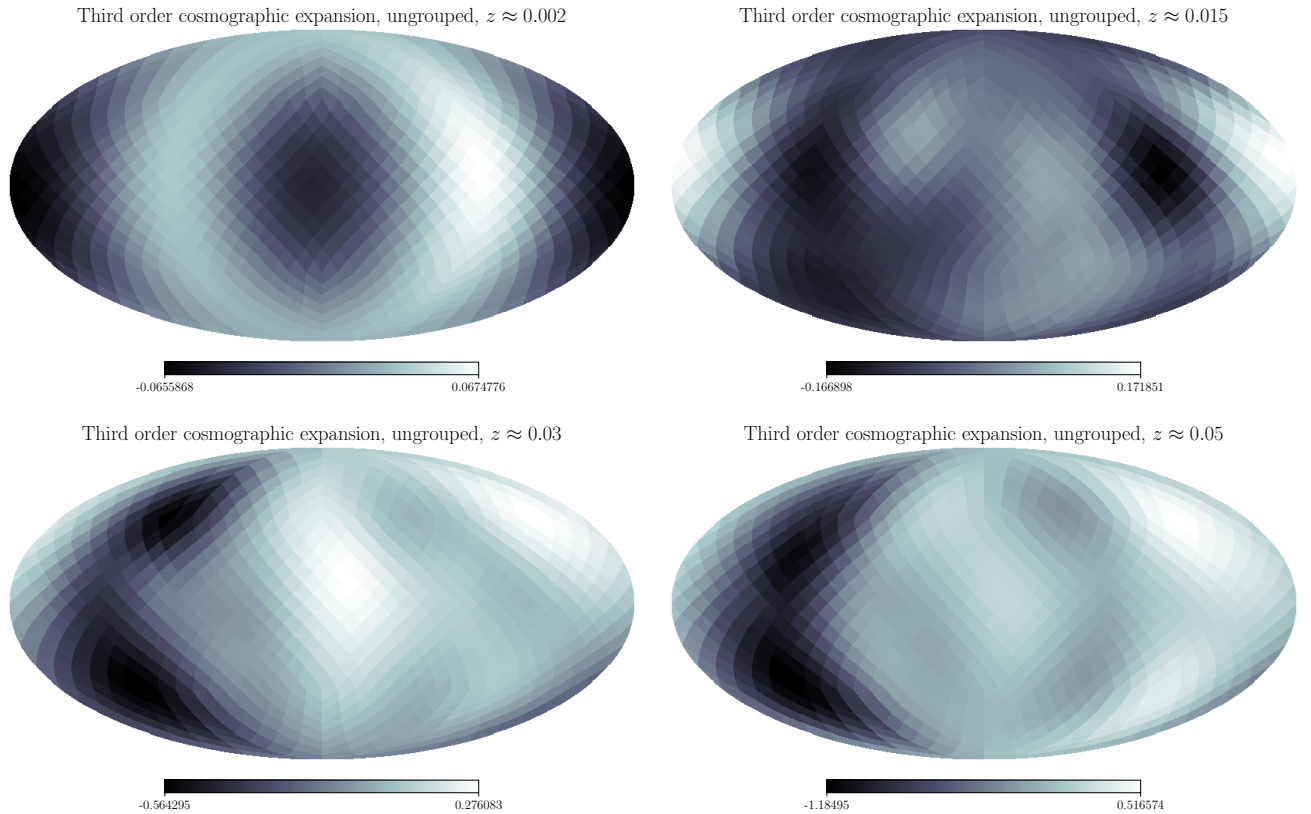


FIG. 4. All-sky maps of the deviation between the exact redshift-distance relation and the third order general cosmographic expansion for the model based on ungrouped data. The deviation is defined as $(D_L - \text{cosmo})/D_L$, where cosmo denotes the cosmographic expansion at third order. The individual plots show the distributions at different redshifts.

For the model based on the grouped data there is a clear asymmetry around zero already at $z = 0.002$ and the asymmetry between negative and positive relative fluctuations are in general more pronounced in the results obtained with the grouped data. Although the amplitudes of the fluctuations are smaller than in the ungrouped case, they are of roughly the same order of magnitude as the fluctuations obtained using the model based on the ungrouped data.

The sky maps show that the light rays along which there is divergence (similar to light ray 2 in the earlier subsection) are assembled in patches in the sky. In these patches, the disagreement between the cosmographic expansion and the exact redshift-distance relation is so significant that the expansion must be considered unsuitable already at $z \approx 0.015$ and above. Between these patches, the cosmographic expansion matches the exact redshift-distance relation much better and could possibly be sensible to use.

Using the general cosmographic expansion rather than the one based on FLRW spacetimes is primarily interesting if the fluctuations of cosmological quantities such as the effective Hubble and deceleration parameters fluctuate significantly across the sky. Next subsection therefore presents all-sky maps of these quantities.

B. Hubble, deceleration, jerk and curvature

In this subsection, sky maps of the Hubble, deceleration and jerk parameters as well as the curvature term are presented.

Figure 6 shows the all-sky distributions of \mathcal{H}_O for the two models. The fluctuations are shown relative to the background Hubble constant of $H_0 = 74.6 \text{ km/s/Mpc}$. For the model based on the ungrouped data, \mathcal{H}_O reaches up to approximately 19% larger than the background value and 11% smaller along the most extreme lines of sight. For the model based on the grouped data, these fluctuations reduce to roughly 11% and 9%, respectively.

The patterns in the sky maps of \mathcal{H}_O resemble the $z \approx 0.005$ sky map of the relative deviations of the cosmographic expansion from the exact redshift-distance relation in figures 4 and 5. However, the strongest amplitude in the fluctuation of \mathcal{H}_O are *not* consistently along the same lines of sight where the cosmographic expansion deviates the most from the exact redshift-distance relation. This could indicate that using the cosmographic expansion only along the lines of sight where the cosmographic expansion converges would still reveal significant fluctuations in \mathcal{H}_O . Similarly, the

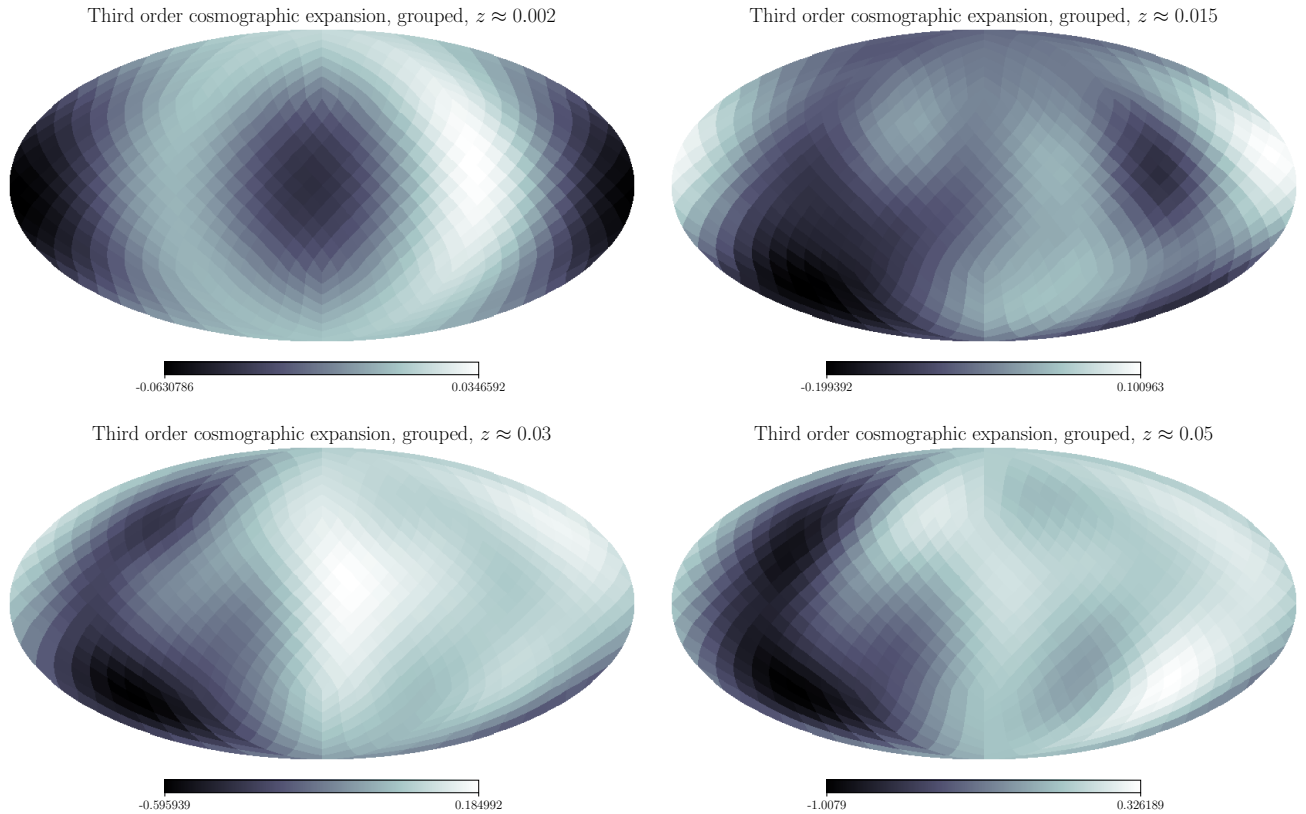


FIG. 5. All-sky maps of the deviation between the exact redshift-distance relation and the third order general cosmographic expansion for the model based on grouped data. The deviation is defined as $(D_L - \text{cosmo})/D_L$, where cosmo denotes the cosmographic expansion at third order. The individual plots show the distributions at different redshifts.

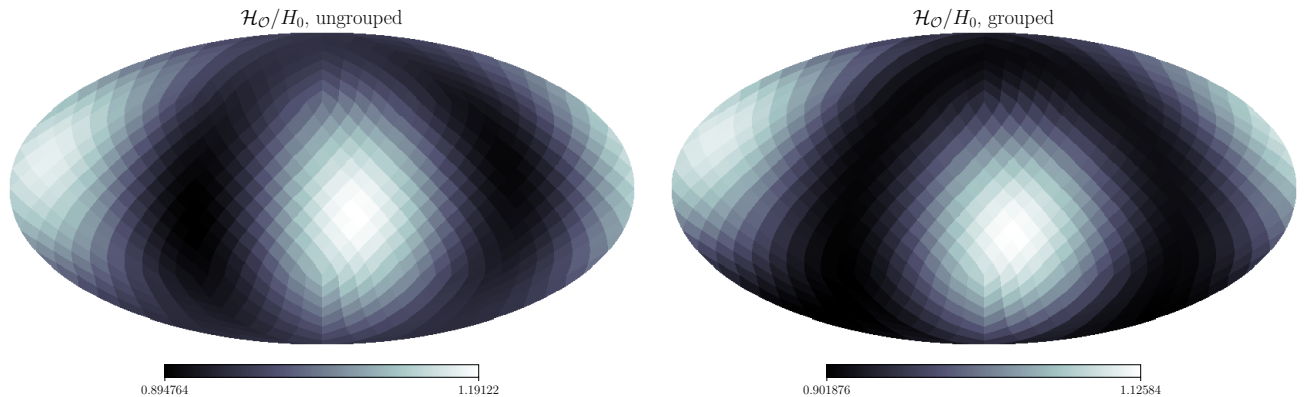


FIG. 6. All-sky maps of \mathcal{H}_O for the considered observer, depicted relative to the background value of H_0 . The sky maps are shown for the models based on both the grouped and ungrouped data.

largest amplitudes in the patterns in the sky maps of \mathcal{Q}_O , \mathcal{J}_O and \mathcal{R}_O do not show a clear correlation with clear divergence of the cosmographic expansion.

Figure 7 shows the all-sky distributions of \mathcal{Q}_O for the two models. \mathcal{Q}_O is shown relative to the background deceleration parameter -0.55 . As seen in figure 7, the values along the 768 lines of sight in the model based

on the ungrouped data fluctuate around the background value by approximately 4000 percent. For the model based on the grouped data, the fluctuations are only slightly smaller.

Figures 8 and 9 shows \mathcal{J}_O and \mathcal{R}_O for both models. The distribution of \mathcal{J}_O runs over 2-3 orders of magnitude larger than the background values of 1. \mathcal{R}_O only

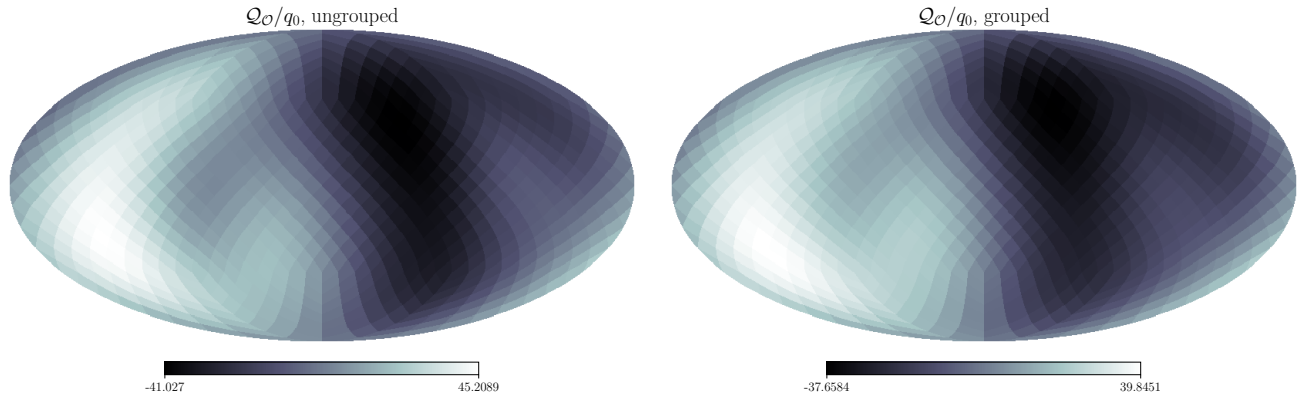


FIG. 7. All-sky maps of $\mathcal{Q}_{\mathcal{O}}$ for the considered observer, depicted relative to the background value, q_0 . The sky maps are shown for the models based on both the grouped and ungrouped data.

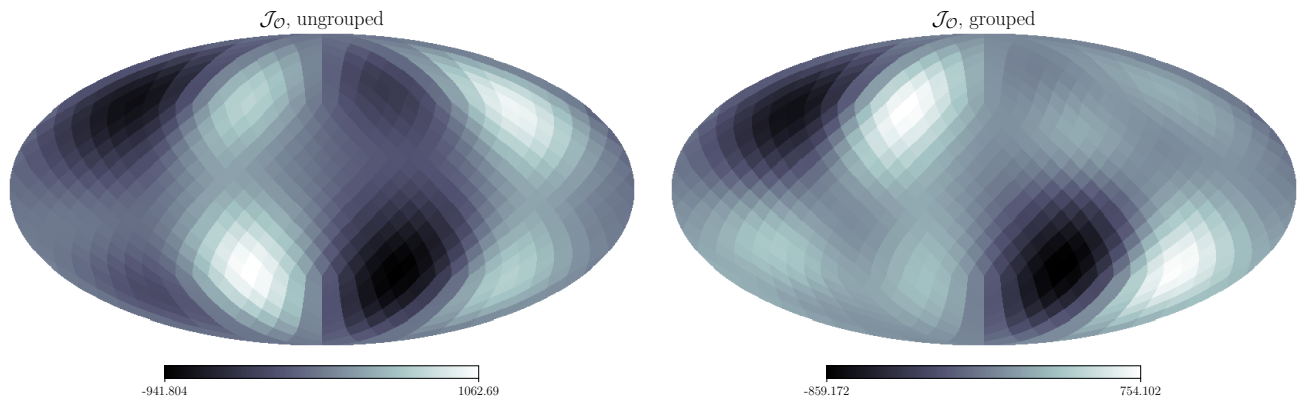


FIG. 8. All-sky maps of $\mathcal{J}_{\mathcal{O}}$ for the considered observer. The sky maps are shown for the models based on both the grouped and ungrouped data.

reaches order of magnitude 10 (while being zero in the background). This is the case both for the model based on the grouped and ungrouped data. In general, the difference in the results obtained from the two models are very small for $\mathcal{H}_{\mathcal{O}}$ and especially $\mathcal{Q}_{\mathcal{O}}$, $\mathcal{J}_{\mathcal{O}}$ and $\mathcal{R}_{\mathcal{O}}$.

Table II shows the mean values of $\mathcal{H}_{\mathcal{O}}$, $\mathcal{Q}_{\mathcal{O}}$, $\mathcal{J}_{\mathcal{O}}$ and $\mathcal{R}_{\mathcal{O}}$ for the 768 lines of sight for the observer in both models. The mean values of $\mathcal{H}_{\mathcal{O}}$ deviate less than 5% from the background value in both models. The deviations are larger for $\mathcal{Q}_{\mathcal{O}}$ but still not alarmingly large. The mean value of $\mathcal{R}_{\mathcal{O}}$ for both models is also fairly small and hence close to its background value of zero. The values of $\mathcal{J}_{\mathcal{O}}$ are somewhat larger, deviating by a factor of over 40 from the background value of 1.

Table II also shows the mean value of the combination $\mathcal{J}_{\mathcal{O}} - \mathcal{R}_{\mathcal{O}} - 1$ which will be discussed in the subsection below, where the results presented here are compared to earlier work.

C. Comparison to earlier work

In [25], the general cosmographic expansion was used in low-resolution simulations with a density contrast amplitude of ~ 0.05 made with the Einstein Toolkit. The authors found that even in such a low resolution simulation, random observers find sky-variance of $\mathcal{H}_{\mathcal{O}}$ of typically 2% and of $\mathcal{Q}_{\mathcal{O}}$ of roughly 120%. The fluctuations found here for $\mathcal{H}_{\mathcal{O}}$ are about a factor of 5-10 higher, depending on whether the grouped or ungrouped data is used. For $\mathcal{Q}_{\mathcal{O}}$, the all-sky fluctuations in $\mathcal{Q}_{\mathcal{O}}$ have a maximum amplitude about of the order of 4000 percent around the background value of -0.55 . This is significantly more than the fluctuations found in [25], but considering that higher density contrasts are used here, this is not particularly troublesome.

In [27], the general cosmographic expansion was recast using the Padé approximant [44] and used in combination with simulations made with gevolution and a randomly placed observer. The main simulation studied had a resolution of 1.75Mpc/h [45], but the

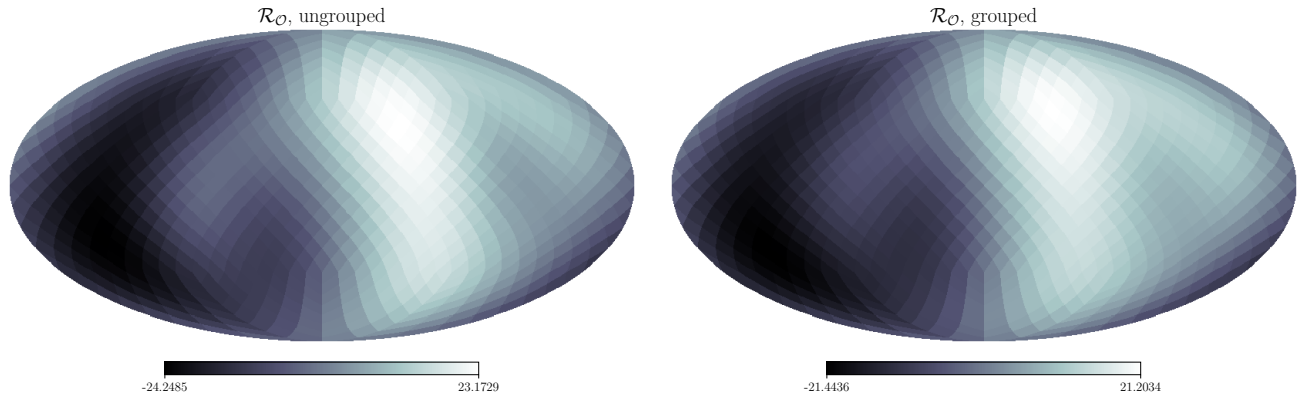


FIG. 9. All-sky maps of \mathcal{R}_O for the considered observer. The sky maps are shown for the models based on both the grouped and ungrouped data.

Model	\mathcal{H}_O (km/s/Mpc)	\mathcal{Q}_O	\mathcal{J}_O	\mathcal{R}_O	$\mathcal{J}_O - \mathcal{R}_O - 1$
Ungrouped	75.5	-0.638	47.7	-0.0511	46.8
Grouped	73.0	-0.518	39.1	-0.0113	38.1
Background	74.5	-0.550	1.00	0.00	0.00

TABLE II. Mean values of \mathcal{H}_O , \mathcal{Q}_O , \mathcal{R}_O and \mathcal{J}_O across the sky for the both models. In addition, the table shows the values of $\mathcal{J}_O - \mathcal{R}_O - 1$ obtained by inserting the mean values of \mathcal{J}_O and \mathcal{R}_O .

study included a comparison with a “smoothed” version of the simulation. From Figures 6-8 in [27] it is seen that the components of the expansions can overall only be constrained accurately/correctly when considering very low redshifts and/or using the smoothed version of the simulation. The only somewhat consistently good results are obtained for the smoothed simulation using data only at $z < 0.025$. This is in line with the results of [26], where it was found that even in a smoothed simulation made with the Einstein Toolkit (equivalent to the smoothed simulation used in [27]), the cosmographic expansion was inaccurate above $\sim 10\%$ for $z > 0.04$. The results of [26] also demonstrate that the accuracy of the cosmographic expansion decreases significantly when the simulations include successively more structure. These results are overall in agreement with the results found here, where the cosmographic expansion is found to break down along a significant portion of the lines of sight long before $z = 0.1$ is reached. By comparing the results based on the grouped-versus-ungrouped data it is also here demonstrated that smoothing (by grouping structures) increases the applicability of the cosmographic expansion, although the effect is quite modest for the two models studied here.

It is worth noting that the results obtained here, in [27] and in [26] are based on different approximations. The approximations made in the current work include the weak field assumption which are also included in the gevolution simulations used in [27]. In [27], perturbations to the light path were neglected together with the Doppler convergence. While the former approximation

was also utilized here, the latter approximation was not since it is well-known that the Doppler convergence is the most important contribution to the convergence at low redshift [39, 41, 42, 45]. The results presented in [27] were additionally obtained by assuming, for simplicity, that $\mathcal{H}_O^3(\mathcal{J}_O - \mathcal{R}_O - 1) = 0$, with the remark that in the Λ CDM model, $\mathcal{J}_O - \mathcal{R}_O - 1 \sim 10^{-4}$. As shown in figure 10, this combination of parameters fluctuates across the sky for both observers with maximum fluctuation amplitude of order $10^2 - 10^3$, i.e. the values found here are up to 10^7 orders of magnitude above the value of the standard Λ CDM model and it is therefore not clear that the constraint $\mathcal{H}_O^3(\mathcal{J}_O - \mathcal{R}_O - 1) = 0$ is viable. In [25, 26], none of the approximations listed here were used. Instead, the redshift and distances were computed according to the exact metric of the simulation. The inhomogeneity of the simulation used in [25, 26] is, however, significantly less than in the other models discussed.

Despite the models studied in [25–27] and here all being quite different, the cosmographic expansion is consistently found to only be valid at very low redshifts, with z of order 0.01 at most, unless structures are smoothed to an amplitude of 0.05.

In [28] the general cosmographic expansion was studied using various LTB models made to mimic our cosmic neighborhood. It was found that the radius of convergence was very low for most of these models and that the second and especially third order cosmographic expansion quickly became very large, leading to the

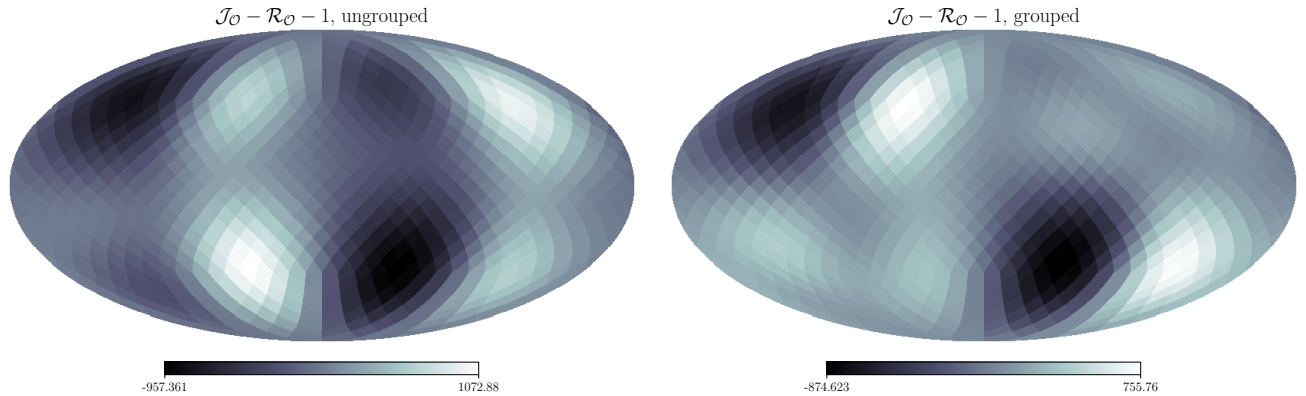


FIG. 10. All-sky maps of $\mathcal{J}_O - \mathcal{R}_O - 1$ for the considered observer. The sky maps are shown for the models based on both the grouped and ungrouped data.

cosmographic expansions deviating by many orders of magnitude from the exact luminosity distance long before $z = 0.1$ was reached. Although the cosmographic expansion is also here found to convergence only at very low redshifts when truncating at third order, the deviations between the cosmographic expansion and the exact luminosity distance are much less significant here than in the most extreme cases found in [28]. The main reason for this is presumably that the gradients of the relevant spacetime quantities were steeper in the given LTB models than in the models studied here. The fluctuations of \mathcal{H}_O , \mathcal{Q}_O , \mathcal{J}_O and \mathcal{R}_O found here are also much smaller than what was found in [28].

V. SUMMARY, DISCUSSION AND CONCLUSIONS

The convergence of the general cosmographic expansion introduced in [17] (see also [18]) was studied in a semi-realistic model of our cosmic neighborhood based on a weak-field approximation combined with CosmicFlows-4 data. By studying the cosmographic expansion along individual lines of sight it was demonstrated that the expansion may be non-diverging up to $z \sim 0.1$ along certain lines of sight. Along other lines of sight, the cosmographic expansion clearly diverges at significantly lower redshift. When considering 768 lines of sight of a single, realistically placed observer, it is clearly seen that the mean of the expansion is dominated by lines of sight along which the expansion diverges already at very low redshifts. This is in line with other similar studies based on less realistic models such as LTB models or simulations with randomly placed observers and various approximations which all find that the cosmographic expansion breaks down at $z \sim 0.01$ or earlier. Only when very small deviations ($\delta \sim 0.05$) from an exactly smooth spacetime is introduced is it possible to achieve accurate approximations using the cosmographic expansion at higher redshift.

Since only the first three coefficients of the cosmographic expansion were considered, the radius of convergence of the cosmographic expansion was not computed explicitly. It is therefore possible that the breakdown of the expansion is not due to a small radius convergence. Instead, the problem may merely be a (very) slow rate of convergence. In this case, obtaining better agreement between the cosmographic expansion and the exact redshift-distance relation simply requires adding more terms in the expansion.

Identifying the exact redshift where the cosmographic expansion is no longer accurate depends both on the given model universe (including its resolution), observer position and line of sight. It would therefore be prudent if applications of general cosmographic expansion schemes were accompanied by explicit studies of the convergence of the expansion in the given model. This is straightforward for studies based on simulation data. For studies based on real data, convergence of the cosmographic expansion can be estimated by making a model similar to those used here, where data was combined with a weak-field approximation.

Even though the cosmographic expansion breaks down at low redshift, the generalized Hubble, deceleration, jerk and curvature parameters can be computed directly for each line of sight. Their validity does not depend on the convergence of the cosmographic expansion. The generalized Hubble constant, \mathcal{H}_O , was found to fluctuate with 10 – 20% compared to the background value while \mathcal{Q}_O was found to fluctuate with an amplitude up to approximately 4000 percent around the background value of $q_0 = -0.55$.

This study confirms that the general cosmographic expansion of the luminosity distance breaks down at very low redshifts for realistically placed observers in realistic density and velocity fields. However, the study also highlights the information we are losing in cosmology by simply applying the FLRW cosmographic expansion. The generalized Hubble, deceleration, jerk

and curvature parameters fluctuate at an order of 10 to over thousands of percent across the sky in the studied, semi-realistic model. This information is erased when utilizing the simple cosmographic expansion based on the FLRW model. It is therefore worth scrutinizing if better convergence of the general cosmographic expansion can be obtained by e.g. recasting it into other forms or by simply including more terms in the expansion. Furthermore, by considering sky maps of the deviations between the exact redshift-distance relation and the cosmographic expansion, it may be possible to single out patches of the sky where the expansion converges at higher redshifts. In addition, other datasets effectively smooth the universe at other scales than the CosmicFlows-4 dataset. Hence, other datasets may have significantly higher radii of convergence and/or faster convergence rates. This could for instance be the case for the Pantheon+ dataset studied with the general cosmographic expansion in [3]. Even the CosmicFlows-4 data used here could be studied at different resolutions to better understand the effects of resolution. Currently, the peculiar velocity and density fields obtained from the CosmicFlows-4 data is only publicly available with a 64^3 -point grid, but grids based on 128^3 and 256^3 grid points also exist and may become publicly available in the future. However, it is actually lower resolution that would lead to better convergence of the cosmographic expansion without adding more expansion terms. The relation between the accuracy of the general cosmographic expansion and the resolution of simulation data was assessed in appendix A of [25] where it was e.g. conjectured that the general cosmographic expansion would be accurate at percent level in the interval $0.04 \lesssim z \lesssim 0.15$ only if the first at least *eight* terms of the expansion were used together with a smoothing scale of $\sim 200\text{Mpc}/h$. Better accuracy can be obtained with fewer terms if the smoothing is done on larger scales and/or smaller redshift intervals are considered.

It is important to note that it is currently unclear how the lack of convergence of the cosmographic expansion actually affects constraints of e.g. \mathcal{H}_O , \mathcal{Q}_O , \mathcal{J}_O and \mathcal{R}_O obtained using the expansion. Moreover, expansion coefficients obtained from a fit of data to the general cosmographic expansion is not useless even if the cosmographic expansion represents the exact redshift-distance relation poorly. The poor convergence rather means that care must be taken when interpreting results, including determining at what scales the coefficients are probing the Universe.

Lastly, in addition to being used for cosmological studies, the general cosmographic expansion may prove useful as a supplement to standard astronomical tools used for studying the very local universe at $z \lesssim 0.01 - 0.001$.

ACKNOWLEDGMENTS

The author thanks Helene Courtois for correspondence and guidance regarding the density and velocity fields of [32] and Asta Heinesen for comments on the manuscript. The GNU Scientific Library⁵ was used for solving ordinary differential equations. An array of Python modules were used for plotting and data handling, including NumPy⁶, Matplotlib⁷, Healpy⁸, Astropy⁹, io¹⁰ and struct¹¹.

The author is funded by VILLUM FONDEN, grant VIL53032.

Appendix A: Expressions for generalized Hubble parameter, deceleration parameter, jerk and spatial curvature term

This appendix serves to explicitly show the expressions used for computing the coefficients for the cosmographic expansion of the luminosity distance.

To compute \mathcal{H} we need expressions for the expansion rate, shear and acceleration. The expansion rate is, for the considered weak-field model, given by

$$\Theta = \nabla_\alpha u^\alpha \approx 3H + \partial_i u^i, \quad (\text{A1})$$

where $u^\alpha \approx (1, v^i)$ at first order (with v^i the peculiar velocities obtained from the CosmicFlows-4 data). The non-vanishing components of the shear are

$$\begin{aligned} \sigma_{ii} &= \frac{2}{3} a^2 \partial_i v^i \\ \sigma_{ij, (i \neq j)} &= \frac{1}{2} a^2 (\partial_i v^j + \partial_j v^i), \end{aligned} \quad (\text{A2})$$

where sums over repeated indexes are *not* implied. The 4-acceleration has components given by

$$\begin{aligned} a_t &= -a a_{,t} \sum (v^i)^2 \\ a_i &= 2a a_{,t} v^i + a^2 (\partial_t v^i + v^j \partial_j v^i), \end{aligned} \quad (\text{A3})$$

where sums *are* implied over repeated indexes.

With the above we can compute \mathcal{H} , \mathcal{Q} and \mathcal{J} . To compute \mathcal{R} we further need

$$\begin{aligned} k^\mu k^\nu R_{\mu\nu} &= \frac{8\pi G}{c^4} \rho k^\mu k^\nu \left(u_\mu u_\nu + \frac{1}{2} g_{\mu\nu} \right) \\ &= \frac{8\pi G \rho}{c^4} (u^\mu k_\nu)^2, \end{aligned} \quad (\text{A4})$$

⁵ <https://www.gnu.org/software/gsl/>

⁶ <https://numpy.org/>

⁷ <https://matplotlib.org/>

⁸ <https://healpy.readthedocs.io/en/latest/>

⁹ <https://www.astropy.org/>

¹⁰ <https://docs.python.org/3/library/os.html>

¹¹ <https://docs.python.org/3/library/struct.html>

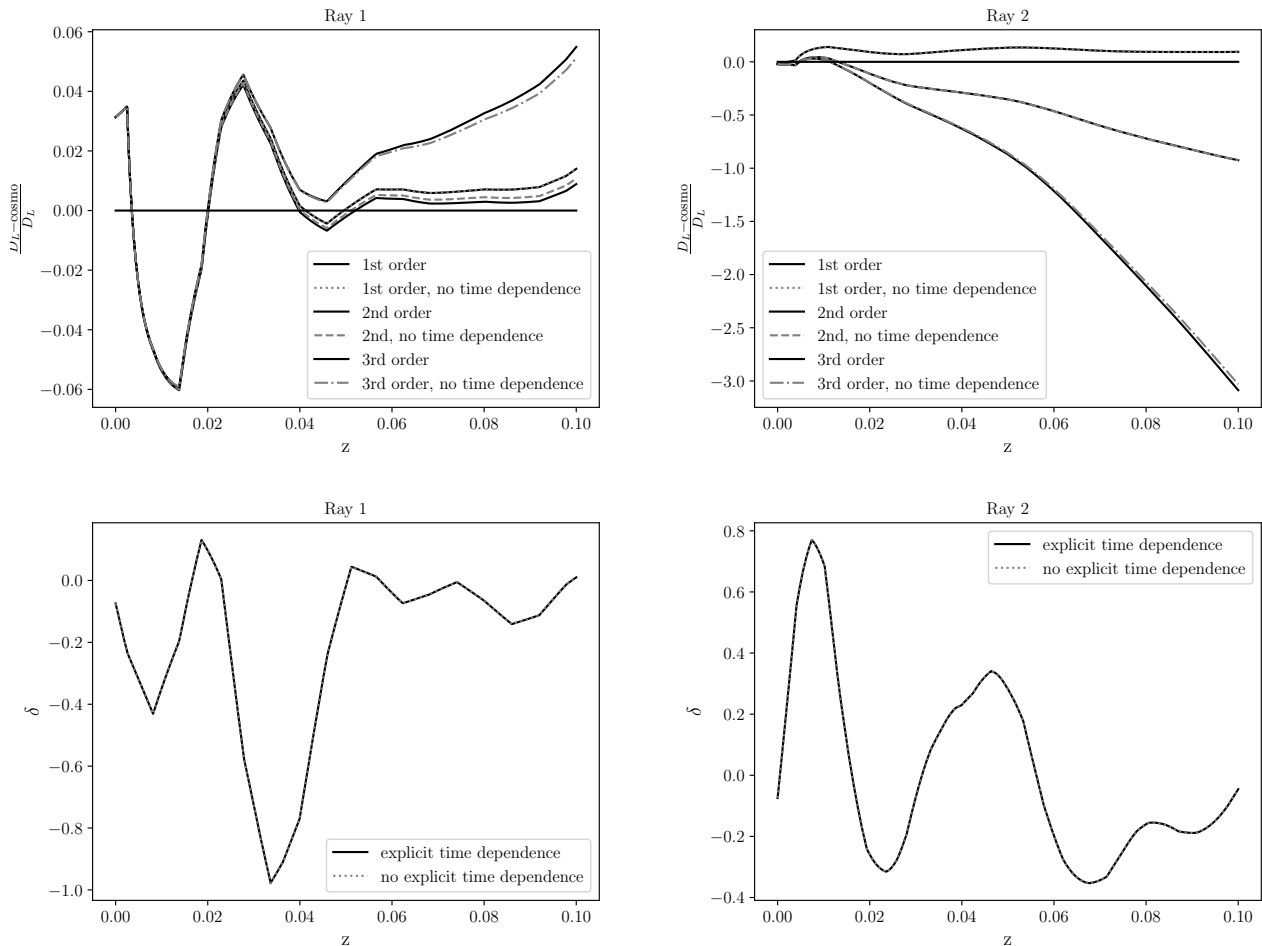


FIG. 11. Density contrast and relative deviations between exact redshift-distance relation and cosmographic expansions (denoted as “cosmo”) along two selected lines of sight. The results are shown for the ungrouped data, comparing results obtained by including versus not including explicit time dependence of v^i and δ . For the density contrasts, it is not possible to distinguish the lines obtained from the two models. For the deviations between exact redshift-distance relation and cosmographic expansions, tiny deviations are visible along some of the lines.

where the first equality comes from employing Einstein’s equation.

Appendix B: Results without time evolution

The results presented in Section IV are based on explicitly including time dependence of δ and v^i by updating these according to $\delta_{,t} = -\delta\Theta$ and $v^i_{,t} = -Hv^i$. This appendix serves to demonstrate the quantitative implications of including this time development, by comparing

with results obtained by neglecting this explicit time development. The results along the two selected light rays studied in Section IV are presented again in Figure 11, this time compared with the equivalent results obtained without including explicit time dependence. To avoid clutter of the figures, the results are only shown for the ungrouped model. As seen, the effect of removing the explicit time dependence is negligible. Most importantly, the explicit time dependence has no impact on the convergence/divergence along the light rays.

-
- [1] Mohamed Rameez, Subir Sarkar, Is there really a Hubble tension?, *Class. Quantum Grav.* 38 (2021) 154005, [arXiv:1911.06456v4](#) [astro-ph.CO]
 [2] Francesco Sorrenti, Ruth Durrer, Martin Kunz, The Dipole of the Pantheon+SH0ES Data,

- JCAP11(2023)054, [arXiv:2212.10328v2](#) [astro-ph.CO]
 [3] Jessica A. Cowell, Suhail Dhawan, Hayley J. Macpherson, Potential signature of a quadrupolar Hubble expansion in Pantheon+ supernovae, *MNRAS* 526, 1482–1494 (2023), [arXiv:2212.13569v1](#) [astro-ph.CO]

- [4] Leandros Perivolaropoulos, On the isotropy of SnIa absolute magnitudes in the Pantheon+ and SH0ES samples, *Phys. Rev. D* 108, 063509 (2023), [arXiv:2305.12819v1](#) [astro-ph.CO]
- [5] Li Tang, Hai-Nan Lin, Liang Liu, Xin Li, Consistency of Pantheon+ supernovae with a large-scale isotropic universe, *Chinese Phys. C* 47 125101, [arXiv:2309.11320v2](#) [astro-ph.CO]
- [6] Ruairi McConville, Eoin O Colgain, Anisotropic Distance Ladder in Pantheon+ Supernovae, *Phys. Rev. D* 108, 123533 (2023), [arXiv:2304.02718v2](#) [astro-ph.CO]
- [7] Jianping Hu, Jian Hu, Xuandong Jia, Baoquan Gao, Fayin Wang, Testing cosmic anisotropy with Pade approximation and Pantheon+ sample, *A&A* 689, A215 (2024), [arXiv:2406.14827v1](#) [astro-ph.CO]
- [8] Carlos A. P. Bengaly, Cassio Pigozzo, Jailson S. Alcaniz, Testing the isotropy of cosmic acceleration with Pantheon+ and SH0ES: A cosmographic analysis, *Phys.Rev.D* 109 (2024) 12, 123533, [arXiv:2402.17741v2](#) [astro-ph.CO]
- [9] J. P. Hu, Y. Y. Wang, J. Hu, F. Y. Wang, Testing the cosmological principle with the Pantheon+ sample and the region-fitting method, *A&A*, 681, A88 (2024), [arXiv:2310.11727v2](#) [astro-ph.CO]
- [10] Animesh Sah, Mohamed Rameez, Subir Sarkar, Christos Tsagas, Anisotropy in Pantheon+ supernovae, [arXiv:2411.10838v1](#) [astro-ph.CO]
- [11] Mohamed Rameez, Anisotropy in the cosmic acceleration inferred from supernovae, [arXiv:2411.14758v1](#) [astro-ph.CO]
- [12] Nathan Secrest, Sebastian von Hausegger, Mohamed Rameez, Roya Mohayaee, Subir Sarkar, A Challenge to the Standard Cosmological Model, *Astrophys. J. Lett.* 937 (2022) L31, [arXiv:2206.05624v2](#) [astro-ph.CO]
- [13] Lawrence Dam, Geraint F. Lewis, Brendon J. Brewer, Testing the Cosmological Principle with CatWISE Quasars: A Bayesian Analysis of the Number-Count Dipole, *MNRAS* 525, 231–245 (2023), [arXiv:2212.07733v2](#) [astro-ph.CO]
- [14] J. D. Wagenfeld, H-R. Klöckner, D. J. Schwarz, The cosmic radio dipole: Bayesian estimators on new and old radio surveys, *A&A* 675, A72 (2023), [arXiv:2305.15335v1](#) [astro-ph.CO]
- [15] G. F. R. Ellis, J. E. Baldwin, On the expected anisotropy of radio source counts, *MNRAS* (1984) 206, 377-381, <https://doi.org/10.1093/mnras/206.2.377>
- [16] Richard Watkins et al., Analyzing the Large-Scale Bulk Flow using CosmicFlows4: Increasing Tension with the Standard Cosmological Model, *MNRAS* 524, 1885–1892 (2023), [arXiv:2302.02028v1](#) [astro-ph.CO]
- [17] Asta Heinesen, Multipole decomposition of the general luminosity distance 'Hubble law' – a new framework for observational cosmology, *JCAP05(2021)008*, [arXiv:2010.06534v2](#) [astro-ph.CO]
- [18] Umeh, O. 2013. The influence of structure formation on the evolution of the universe. University of Cape Town (PhD thesis)
- [19] Roy Maartens, Jessica Santiago, Chris Clarkson, Basheer Kalbouneh, Christian Marinoni, Covariant cosmography: the observer-dependence of the Hubble parameter, *JCAP09(2024)070*, [arXiv:2312.09875v3](#) [astro-ph.CO]
- [20] Basheer Kalbouneh, Christian Marinoni, Roy Maartens, Cosmography of the Local Universe by Multipole Analysis of the Expansion Rate Fluctuation Field, [arXiv:2401.12291v1](#) [astro-ph.CO]
- [21] Basheer Kalbouneh, Jessica Santiago, Christian Marinoni, Roy Maartens, Chris Clarkson, Maharshi Sarma, Expanding covariant cosmography of the local Universe: incorporating the snap and axial symmetry, [arXiv:2408.04333v1](#) [astro-ph.CO]
- [22] Chris Clarkson, Obinna Umeh, Is backreaction really small within concordance cosmology?, *Class. Quantum Grav.* 28 164010 (2011), [arXiv:1105.1886v1](#) [astro-ph.CO]
- [23] Stella Seitz, Peter Schneider, Juergen Ehlers, Light Propagation in Arbitrary Spacetimes and the Gravitational Lens Approximation, *Class.Quant.Grav.*11:2345-2374,1994, [arXiv:astro-ph/9403056v1](#)
- [24] G.F.R. Ellis, S.D. Nel, R. Maartens, W.R. Stoeger, A.P. Whitman, Ideal observational cosmology, *Physics Reports*, Volume 124, Issues 5–6, July 1985, Pages 315-417
- [25] Hayley J. Macpherson, Asta Heinesen, Luminosity distance and anisotropic sky-sampling at low redshifts: a numerical relativity study, *Phys. Rev. D* 104, 023525 (2021), [arXiv:2103.11918v3](#) [astro-ph.CO]
- [26] Hayley J. Macpherson, Cosmological distances with general-relativistic ray tracing: framework and comparison to cosmographic predictions, *JCAP03(2023)019*, [arXiv:2209.06775v2](#) [astro-ph.CO]
- [27] Julian Adamek, Chris Clarkson, Ruth Durrer, Asta Heinesen, Martin Kunz, Hayley J. Macpherson, Towards Cosmography of the Local Universe, *The Open Journal of Astrophysics* 7 (2024), [arXiv:2402.12165v2](#) [astro-ph.CO]
- [28] Asha B. Modan, S. M. Koksbang, On the convergence of cosmographic expansions in Lemaitre-Tolman-Bondi models, *Class. Quantum Grav.* 41 235018 (2024), [arXiv:2408.07459v2](#) [gr-qc]
- [29] G. Lemaitre: L'Univers en expansion, *Annales de la Societe Scientifique de Bruxelles A* 53, 51 (1933), English translation: The expanding universe, *Gen. Rel. Grav.* 29, 637 (1997)
- [30] R. C. Tolman: Effect of Inhomogeneity on Cosmological Models, *Proc. Natl. Acad. Sci. USA* 20, 169-176 (1934)
- [31] H. Bondi: Spherically Symmetrical Models in General Relativity, *Month. Not. Roy. Astr. Soc.* 107,410 (1947)
- [32] H. M. Courtois, A. Dupuy, D. Guinet, G. Baulieu, F. Ruppin, P. Brenas, Gravity in the Local Universe : density and velocity fields using CosmicFlows-4, *A&A* 670, L15 (2023), [arXiv:2211.16390v4](#) [astro-ph.CO]
- [33] R. Brent Tully et al., Cosmicflows-4, 2023 *ApJ* 944 94, [arXiv:2209.11238v2](#) [astro-ph.CO]
- [34] Aurelien Valade, Noam I. Libeskind, Daniel Pomarede, R. Brent Tully, Yehuda Hoffmann, Simon Pfeifer, Ehsan Kourkchi, Identification of Basins of Attraction in the Local Universe, *Nat. Astron.* (2024), [arXiv:2409.17261v1](#) [astro-ph.CO]
- [35] R. Graziani, H. M. Courtois, G. Lavaux, Y. Hoffman, R. B. Tully, Y. Copin, D. Pomarede, The peculiar velocity field up to $z \sim 0.05$ by forward-modeling Cosmicflows-3 data, *MNRAS* 488, 5438–5451 (2019), [arXiv:1901.01818v1](#) [astro-ph.CO]
- [36] Julian Adamek, David Daverio, Ruth Durrer, Martin Kunz, gevolution: a cosmological N-body code based on General Relativity, *JCAP* 1607 (2016) no.07, 053, [arXiv:1604.06065v2](#) [astro-ph.CO]
- [37] S. R. Green and R. M. Wald, Newtonian and Relativistic Cosmologies, *Phys. Rev. D*85 (2012) 063512, [arXiv:1111.2997](#)

- [38] S. M. Kocsbang, S. Hannestad, Methods for studying the accuracy of light propagation in N-body simulations, *Phys. Rev. D* 91, 043508 (2015), [arXiv:1501.01413v3](#) [astro-ph.CO]
- [39] S. M. Kocsbang, S. Hannestad, Studying the precision of ray tracing techniques with Szekeres models, *Phys. Rev. D* 92, 023532 (2015), [arXiv:1506.09127v3](#) [astro-ph.CO]
- [40] George F. R. Ellis, Roy Maartens and Malcolm A. H. MacCallum, *Relativistic Cosmology*, Cambridge University Press, ISBN 978-0-521-38115-4, 2012
- [41] Krzysztof Bolejko, Chris Clarkson, Roy Maartens, David Bacon, Nikolai Meures, Emma Beynon, Anti-lensing: the bright side of voids, *Phys. Rev. Lett.* 110, 021302 (2013), [arXiv:1209.3142v3](#) [astro-ph.CO]
- [42] Camille Bonvin, Effect of Peculiar Motion in Weak Lensing, *Phys.Rev.D*78:123530,2008, [arXiv:0810.0180v3](#) [astro-ph]
- [43] R. Sachs, *Gravitational Waves in General Relativity*. VI. The Outgoing Radiation Condition, *Proceedings of the Royal Society of London Series A*, 264(1318):309–338 (1961)
- [44] Hao Wei, Xiao-Peng Yan, Ya-Nan Zhou, Cosmological Applications of Pade Approximant, *JCAP*1401:045,2014, [arXiv:1312.1117v3](#) [astro-ph.CO]
- [45] Louis Coates, Julian Adamek, Philip Bull, Caroline Guandalin, Chris Clarkson, Observing relativistic features in large-scale structure surveys – II: Doppler magnification in an ensemble of relativistic simulations, *MNRAS*,504(3),2021,3534-3543, [arXiv:2011.12936v2](#) [astro-ph.CO]